IL NUOVO CIMENTO VOL. 107 A, N. 9 Settembre 1994

Scattering of Alpha-Particles from ^{46}Ti at $E_\alpha = 45$ and 50 MeV and from ^{48}Ti at $E_\alpha = 40$ and 45 MeV.

V. RAGHUNATHA RAO (1) (*), M. SUDARSHAN (1) (**), A. SARMA (1) (***)
R. SINGH (1), S. R. BANERJEE (2) and S. N. CHINTALAPUDI (2) (**)

(1) *Physics Department, North-Eastern Hill University - Shillong 793003, India*
(2) *Variable Energy Cyclotron Centre, BARC - 1/AF Bidhan Nagar, Calcutta 700064, India*

(ricevuto il 16 Settembre 1993; approvato il 3 Novembre 1993)

Summary. — Differential cross-sections for elastic and inelastic scattering of 45 and 50 MeV alpha-particles from ^{46}Ti have been measured in the angular range from $\theta_{lab} = 5°$ to 135° in 2.5° and 5° steps and those of 40 and 45 MeV alpha-particles from ^{48}Ti in the angular ranges from $\theta_{lab} = 20°$ to 125° and 5° to 130°, respectively, in the same angular steps. A six-parameter optical-model analysis of the elastic-scattering data has been carried out using Woods-Saxon, and Woods-Saxon–squared radial dependences. A method based on predicting optical-model potential parameters starting with a consistent set of parameters at higher energies following the energy dependences established from the systematics has also been used. The most sensitive region of the potential in predicting the elastic-scattering cross-sections has been found by using a notch perturbation test. The problem of discrete family ambiguity in the optical-model analysis of elastic data has also been investigated. The inelastic-scattering data have been analysed in terms of the collective model using the distorted-wave Born approximation (DWBA), where the distorted waves are generated by the optical potential obtained from the elastic-scattering data. The values of the deformation parameter (β_2) thus obtained compare very well with the ones reported earlier.

PACS 25.55 – ^{3}H-, ^{3}He- and ^{4}He-induced reactions and scattering.
PACS 25.55.Ci – Elastic and inelastic scattering.

1. – Introduction.

Scattering of alpha-particles from Ti-isotopes has been studied in the past [1-5]. Elastic-scattering angular distributions for these and some other nuclei have been

(*) Present address: Physics Department, St. Edmund's College, Shillong 793003, India.
(**) Present address: Inter University Consortium for DAE Facility, 2/BJ Bidhan Nagar, Calcutta 700064, India.
(***) Present address: Nuclear Science Centre, P.O. Box No. 10502, New Delhi, India.

successfully described with Woods-Saxon squared and other non-standard forms of optical potential over a wide angular and energy range [6-8].

In this paper we present results of our measurements on elastic and inelastic scattering of alpha-particles from ^{46}Ti at $E_\alpha = 45$ and 50 MeV and from ^{48}Ti at $E_\alpha = 40$ and 45 MeV. The elastic data have been analysed in terms of the optical model with Woods-Saxon and Woods-Saxon–squared type of radial dependences. The optical-model parameters were also obtained from the systematics of the volume integrals [9, 10]. These data can help to reduce the ambiguities in the optical-model parameters. A notch perturbation test [11] was carried out for determining the radial region of sensitivity in predicting the elastic scattering. The inelastic-scattering data (for the 0.889 MeV, 2^+ excited state of ^{46}Ti, and 0.983 MeV, 2^+ excited state of ^{48}Ti) have been analysed in terms of collective model using distorted-wave Born approximation.

2. – Experimental procedure.

The experiment was carried out at the Variable Energy Cyclotron Centre, Bhabha Atomic Research Centre, Calcutta, using an unanalysed alpha beam (with an energy spread of $\sim 0.5\%$) from the 224 cm cyclotron. Self-supporting target foils of ^{46}Ti and ^{48}Ti (having thicknesses of 1.080 mg cm^{-2} and 0.965 mg cm^{-2}, and enrichments of 81.02% and 99.25%, respectively) were appropriately mounted at the centre of the 91.5 cm diameter scattering chamber. The target thicknesses were measured both by weighing and by measuring the energy loss of 5.5 MeV alpha-particles from ^{241}Am source. Other experimental conditions were the same as described in our earlier paper [5]. In case of ^{46}Ti the cross-sections include contributions from scattering on ^{48}Ti (present in the target) too as the energy resolution was not sufficient to separate the latter. Thus, the enrichment (81.02%) of the ^{46}Ti target was appropriately accounted for in the thickness, but no corrections were made to the scattered yields. The elastic- and inelastic-scattering angular distributions from ^{46}Ti were measured in the angular range from 5° to 135° in steps of 2.5–5°, and those from ^{48}Ti were measured from 20° to 125° at 40 MeV, and from 5° to 130° at 45 MeV in steps of 2.5–5°. The overall errors in the cross-sections due to uncertainities in the target thickness, integrated charge, and solid angle are estimated, including the counting statistics, to range from ~ 5 to 11%. At some larger angles these errors come up to $\sim 16\%$, primarily due to low-counting statistics. The errors in the data are shown wherever they exceed the size of the point.

3. – Results and discussion.

3·1. *Elastic scattering.* – The elastic-scattering angular distributions exhibit pronounced oscillations for both the isotopes (see fig. 1-4). An optical-model analysis of the data was carried out using a six-parameter (excluding m and n) potential of the following form:

$$V(r) = V_C(r, R_C) - V_R[f(r, r_R, a_R)]^m - iV_I[f(r, r_I, a_I)]^n , \tag{1}$$

where $V_C(r, R_C)$ is the Coulomb potential due to a uniformly charged sphere of radius $R_C = 1.3A_T^{1/3}$ fm; V_R, V_I and A_T are the strengths of the real and imaginary parts,

and the target mass number, respectively. The Woods-Saxon form factors are represented by

$$f(r, r_x, a_x) = [1 + \exp[(r - R_x)/a_x]]^{-1}, \tag{2}$$

where

$$R_x = r_x A_T^{1/3}, \qquad x = \mathrm{R} \text{ or } \mathrm{I}.$$

Here r_x and a_x are the corresponding radius and diffuseness parameters, respectively. The form factor powers m and n are permitted to assume integer values 1 and 2. Besides performing an optical-model analysis similar to what has been described in our earlier paper [5], we used a procedure of extrapolating to lower energies the «unique» potential parameters determined at higher energies with appropriate energy variation [10]. The parameters thus obtained along with χ^2-values, strong-absorption radius (see eq. (3)) and total reaction cross-section are given in tables I and II. For the real part of the potential, the systematics of the volume integral J_R [9], the radius $R_{2.4}$ (where the potential becomes 2.4 MeV) and the slope S of the potential at $R_{2.4}$ were used. For the imaginary part of the potential, the systematics of the volume integral J_I [10], and the ratio of the geometrical parameters $R_{IR} (= R_I/R_R = a_I/a_R)$ were used. Starting with

TABLE I. – *Optical-model parameters deduced from elastic-scattering angular distributions using standard and non-standard Woods-Saxon potential, form factor powers* (m, n), χ^2 *per degree of freedom, strong-absorption radii* ($R_{s.a.}$) *and total reaction cross-sections* (σ_t).

Set	V_R (MeV)	r_R (fm)	a_R (fm)	V_I (MeV)	r_I (fm)	a_I (fm)	(m, n)	χ^2	$R_{s.a.}$ (fm)	σ_t (b)
$\alpha + ^{46}$Ti at $E_\alpha = 45$ MeV										
*A*1	185.63	1.390	0.575	30.37	1.492	0.444	(1, 1)	16.11	7.476	1.416
*B*1	217.45	1.449	0.500	39.23	1.453	0.343	(1, 2)	15.49	—	1.415
*C*1	162.58	1.549	0.920	80.32	0.842	0.859	(2, 1)	19.05	—	1.477
*D*1	292.52	1.457	0.972	29.19	1.560	0.739	(2, 2)	13.21	—	1.411
$\alpha + ^{46}$Ti at $E_\alpha = 50$ MeV										
*E*1	98.10	1.599	0.489	26.23	1.577	0.356	(1, 1)	11.05	7.575	1.471
*F*1	209.23	1.499	0.485	49.40	1.494	0.359	(1, 2)	11.24	—	1.475
*G*1	183.89	1.628	0.810	80.46	1.293	0.459	(2, 1)	12.48	—	1.479
*H*1	234.33	1.603	0.802	50.72	1.414	0.719	(2, 2)	12.66	—	1.476
$\alpha + ^{48}$Ti at $E_\alpha = 40$ MeV										
*I*1	154.10	1.337	0.617	28.31	1.321	0.722	(1, 1)	29.25	7.648	1.475
*J*1	173.99	1.468	0.499	34.50	1.454	0.221	(1, 2)	29.04	—	1.408
*K*1	268.14	1.483	0.945	25.69	1.665	0.287	(2, 1)	21.03	—	1.409
*L*1	267.73	1.484	0.944	25.82	1.665	0.572	(2, 2)	21.03	—	1.409
$\alpha + ^{48}$Ti at $E_\alpha = 45$ MeV										
*M*1	219.02	1.453	0.522	26.95	1.644	0.299	(1, 1)	18.04	7.636	1.482
*N*1	214.33	1.478	0.485	36.97	1.469	0.300	(1, 2)	18.82	—	1.467
*O*1	152.91	1.606	0.912	21.64	1.667	0.337	(2, 1)	17.23	—	1.479
*P*1	257.70	1.540	0.883	24.93	1.651	0.590	(2, 2)	16.16	—	1.467

TABLE II. – *Optical-model parameters deduced from elastic-scattering angular distributions using systematics of volume integrals, χ^2 per degree of freedom and total reaction cross-sections (σ_t).*

Set	V_R (MeV)	r_R (fm)	a_R (fm)	V_I (MeV)	r_I (fm)	a_I (fm)	χ^2	σ_t (b)
$\alpha + {}^{46}$Ti at $E_\alpha = 45$ MeV								
A2	97.29	1.426	0.646	15.71	1.649	0.463	29.98	1.427
$\alpha + {}^{46}$Ti at $E_\alpha = 50$ MeV								
B2	68.06	1.656	0.473	15.60	1.640	0.471	14.49	1.501
$\alpha + {}^{48}$Ti at $E_\alpha = 40$ MeV								
C2	110.63	1.407	0.616	14.76	1.652	0.454	40.53	1.419
$\alpha + {}^{48}$Ti at $E_\alpha = 45$ MeV								
D2	102.21	1.390	0.653	15.41	1.647	0.462	36.71	1.436

these parameters, we optimized the fits to the data by fine-tuning the parameters to get the minimum χ^2-values.

The fits to the ^{46}Ti data at 45 and 50 MeV with standard optical model are shown in fig. 1 and 2. At $E_\alpha = 45$ MeV the standard Woods-Saxon form provides a good

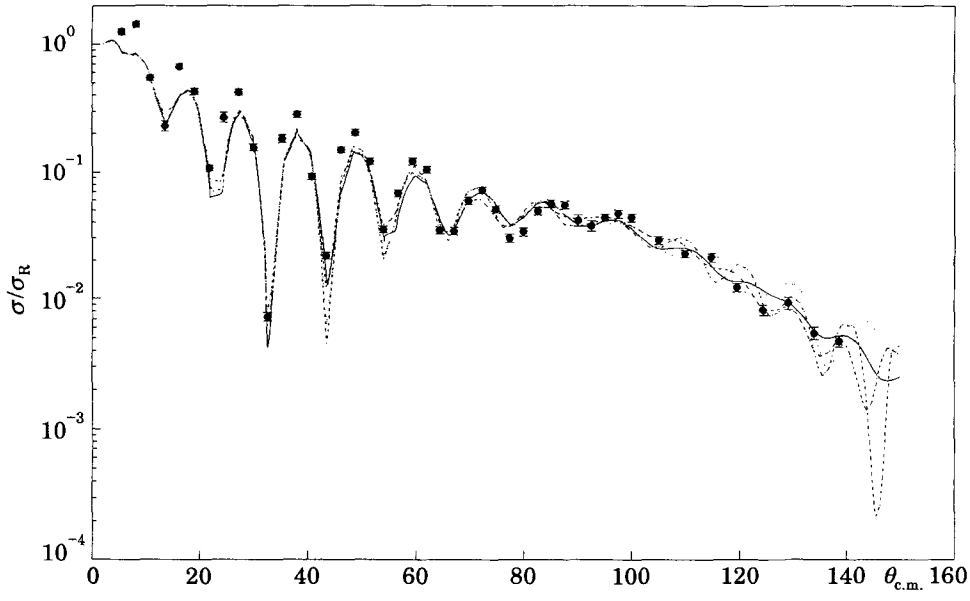

Fig. 1. – The ratio of the differential elastic cross-section to the Rutherford cross-section plotted as a function of centre-of-mass angle along with the fits obtained using standard and non-standard forms of the optical-model potentials for $\alpha + {}^{46}$Ti at $E_\alpha = 45$ MeV. The solid curve corresponds to potential set *A*1, dotted curve to set *B*1, long-dashed curve to set *C*1 and the dashed-dot curve to set *D*1 of table I.

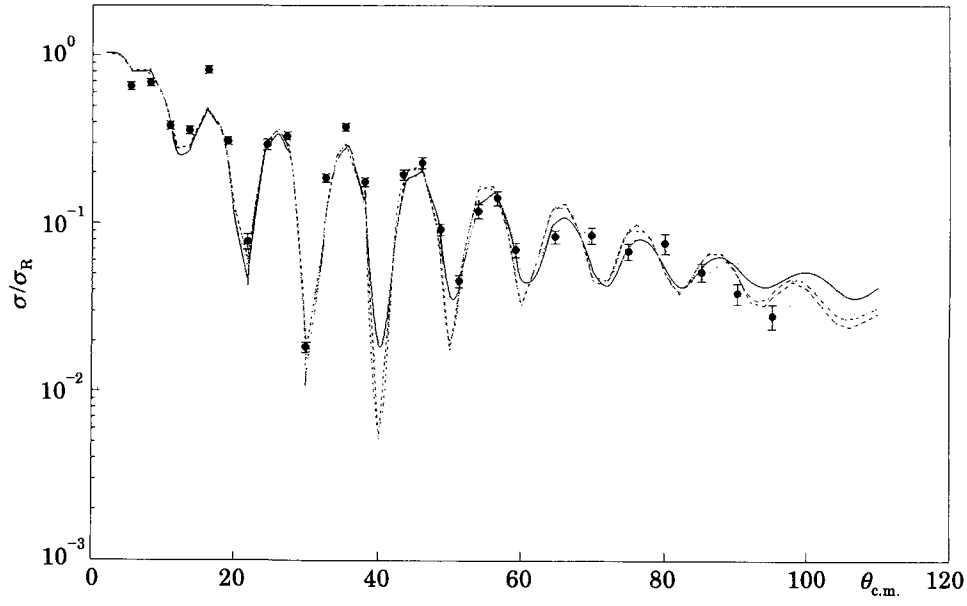

Fig. 2. – The same as fig. 1, but at $E_\alpha = 50$ MeV. The solid curve corresponds to potential set $E1$, dotted curve to set $F1$, long-dashed curve to set $G1$ and the dash-dotted curve to set $H1$ of table I.

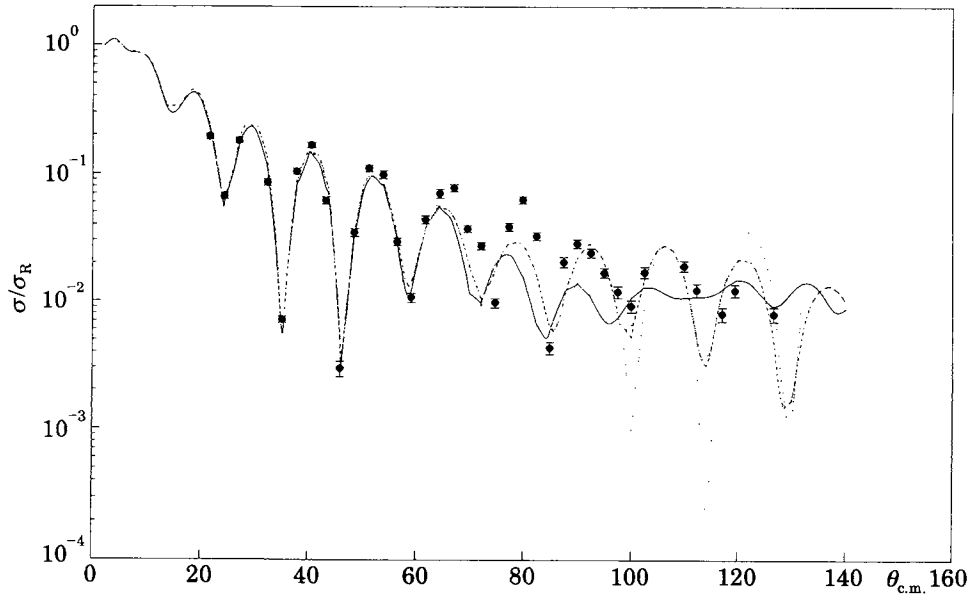

Fig. 3. – The ratio of the differential elastic cross-section to the Rutherford cross-section plotted as a function of centre-of-mass angle along with the fits obtained using standard and non-standard forms of the optical-model potentials for $\alpha + {}^{48}$Ti at $E_\alpha = 40$ MeV. The solid curve corresponds to potential set $I1$, dotted curve to set $J1$, long-dashed curve to set $K1$ and the dashed-dot curve to set $L1$ of table I.

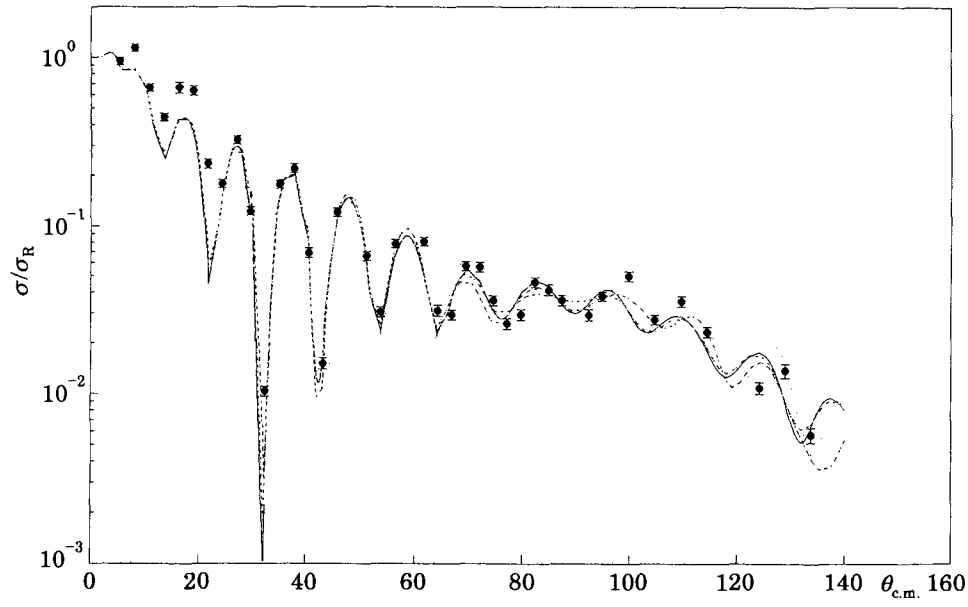

Fig. 4. – The same as fig. 3, but at $E_\alpha = 45$ MeV. The solid curve corresponds to potential set $M1$, dotted curve to set $N1$, long-dashed curve to set $O1$ and the dash-dotted curve to set $P1$ of table I.

description of the data, particularly beyond $\sim 60°$ or so (see fig. 1). At $E_\alpha = 50$ MeV also the standard potential gives a good description of the data up to $\sim 80°$ or so (see fig. 2).

For ^{48}Ti nucleus the data at $E_\alpha = 40$ MeV, the standard optical model describes the data reasonably well up to $\sim 60°$, as can be noted from fig. 3. However, at $E_\alpha = 45$ MeV a similar potential describes the data quite well more or less over the entire angular range (see fig. 4).

The non-standard Woods-Saxon radial dependence of the potential ($m = 1$, $n = 2$; and $m = n = 2$) gave somewhat better description of the ^{46}Ti data at $E_\alpha = 45$ MeV. The $m = n = 2$ combination, of course, gives the best fit. At $E_\alpha = 50$ MeV for ^{46}Ti $m = 1$, $n = 2$ combination gives the best representation of the data, although $m = 2$, $n = 1$, and $m = n = 2$ combinations also give more or less similar qualities of fits. All this can be noted from fig. 1 and 2.

For ^{48}Ti at $E_\alpha = 40$ MeV the non-standard forms $\{m = 1, n = 2$ (up to $\sim 95°$); $m = 2, n = 1$; $m = n = 2\}$ gave better representations of the data as compared to the standard optical potential. Of all of them, of course, $m = 2$, $n = 1$ and $m = n = 2$ combinations describe the data best (see fig. 3). Of course, the quality of fits beyond $\theta_{c.m.} \sim 70°$ is generally not good. The quality of fits for $m = 1$, $n = 2$; $m = 2$, $n = 1$; $m = n = 2$ combinations at $E_\alpha = 45$ MeV was relatively better. Of course, $m = n = 2$ combination gave by far the best fit (see fig. 4). The better description of the elastic data with the non-standard forms of the radial dependence of the optical potential is in conformity with other α-scattering studies in this mass region [4-8] at different energies. It must be mentioned that a better representation of data by using Woods-Saxon squared form for the real part was also noted by Robertson *et al.* [4] for ^{46,48,50}Ti at $E_\alpha = 140$ MeV, by Pesl *et al.* [8] for ^{48}Ca, ^{50}Ti and ^{52}Cr at $E_\alpha = 104$ MeV, and

by Gubler *et al.* [7] for ^{50}Ti and ^{52}Cr in a broad energy range. In a separate analysis of $\alpha + ^{40}$Ca data Gubler *et al.* [12] noted that an optical potential with real part raised to the power 2.65 closely resembled the corresponding folding potential. Thus, the Woods-Saxon squared type of potential might as well be a physically reasonable form for providing good fits to the elastic data.

The strong-absorption radii for $\alpha + ^{46,48}$Ti interactions were calculated using the relation [10]

$$R_{\text{s.a.}} = (\eta/k)[1 + \{1 + (l_{\text{s.a.}} + 1/2)^2/\eta^2\}^{1/2}], \tag{3}$$

where $l_{\text{s.a.}}$ is the value of the orbital angular momentum for which the transmission coefficient becomes 0.5, η is the Sommerfeld parameter and k is the wave number. The values of various parameters including the $R_{\text{s.a.}}$ are given in table I. It can be noted that the values of $R_{\text{s.a.}}$ compare very well with the values 7.692 fm (^{46}Ti) and 7.711 fm for ^{48}Ti at 42 MeV [1].

3·1.1. Notch perturbation test. Notch perturbation test was carried out for investigating the radial sensitivity of the optical potential for elastic scattering [11]. By following the same procedure as described in [5], χ^2-values were calculated (separately for real and imaginary parts) by varying R_{p} (the position of the centre of the notch) from 3 to 9 fm in steps of 0.5 fm. The potential was multiplied by a perturbing factor (R for real part, I for imaginary part) as follows:

$$V_{\text{p}}(r) = V_{\text{R(I)}} f_{\text{R(I)}}[1 - 4d f_{\text{p}}(r)\{1 - f_{\text{p}}(r)\}], \tag{4}$$

with $d = 1$ and

$$f_{\text{p}}(r) = [1 + \exp[(r - R_{\text{p}})/a_{\text{p}}]]^{-1}. \tag{5}$$

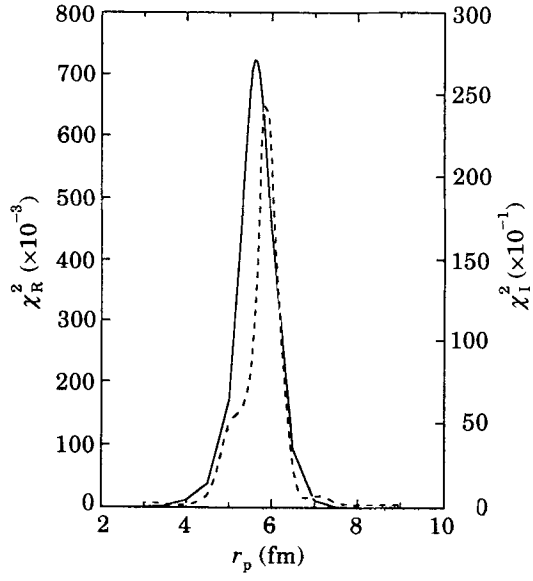

Fig. 5. – The notch perturbation test: the χ^2-values plotted as a function of the notch radius for real (solid curve) and imaginary (dotted curve) parts of the potential for $\alpha + ^{46}$Ti at E_α = = 45 MeV.

The value of a_p was fixed at 0.1 fm for both the real and imaginary parts. The R_p values at which χ^2-maxima occur are 5.6 fm (real), 5.85 fm (imaginary) at 45 MeV and 5.75 fm (real), 6.25 fm (imaginary) at 50 MeV for $\alpha + {}^{46}$Ti. Similarly, for $\alpha + {}^{48}$Ti at 40 and 45 MeV these quantities are 5.65 fm, 6.15 fm and 5.90 fm and 6.10 fm, respectively. Thus it is evident that χ^2-maxima occur well within the strong-absorption radii $R_{s.a.}$ for both the isotopes and at all the four energies. The plots of χ^2-values as a function of notch radius R_p for real and imaginary parts for ^{46}Ti at $E_\alpha = 45$ MeV are shown in fig. 5. From this figure it can be noted that ^{46}Ti nucleus appears effectively black to the 45 MeV α-particles within the first 4 fm of the radius. Similar behaviour was noted for the $\alpha + {}^{46}$Ti at 50 MeV, and for $\alpha + {}^{48}$Ti at 40 and 45 MeV. A comparison of the predicted angular distributions with the perturbed potential having corresponding notch radii equal to the ones having the maximum χ^2-values with the ones obtained by using the unperturbed potential shows that the main angular region of sensitivity is for the angles beyond $\sim 40°$ in all the four cases.

3·1.2. Discrete potential family ambiguities. The existence of discrete family ambiguities in the optical-model analysis of low-energy elastic scattering is well known. Therefore, the real part of the potential cannot really be determined uniquely. It is possible to obtain several discrete potentials which provide equally good fits to the data. However, the number of such potential families can be reduced to a few with the availability of the data over a wide angular range. The possible allowed potential families were determined from the present data. The best-fit potential with standard Woods-Saxon form ($m = n = 1$) was taken as the zeroth family ($N = 0$) and the potentials for $N = \pm 1$ etc. families were obtained as described in ref. [5].

The χ^2-values for various potential families including the ones which do not satisfy the family ambiguity condition were calculated. The results for ^{46}Ti at $E_\alpha = 45$ MeV are presented in fig. 6. These data permit four families. Similar analysis for $\alpha + {}^{46}$Ti at $E_\alpha = 50$ MeV permitted 4, and for $\alpha + {}^{48}$Ti at $E_\alpha = 40$ and 45 MeV permitted 3 and 5

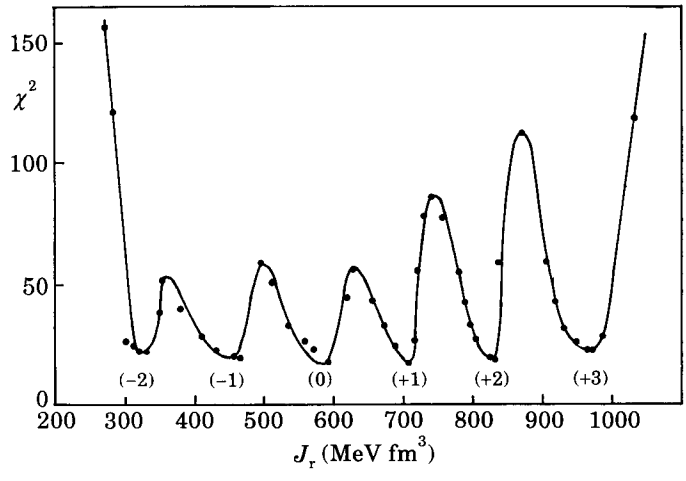

Fig. 6. – Variation of the χ^2 per point as a function (for the $\alpha + {}^{46}$Ti at $E_\alpha = 45$ MeV) of the volume integral of the real potential (J_r). The labels (−2), (−1), (0), (+1), (+2), (+3) represent different discrete potential families discussed in the text.

families, respectively. As expected, there are large χ^2-values (the maximum-to-minimum χ^2-values ratios ranging from 1.7 to 2.9) in between the various families.

3·1.3. Energy dependence of optical-model parameters. In order to have an idea about the energy dependence of the strengths of real and imaginary parts of the optical potential for $\alpha + ^{46,48}$Ti we used the data at 35 MeV [5], 104 MeV [2] and 140 MeV [4] along with the present data and arrived at the following type of energy dependence for the real part:

$$V_R = (152.5 - 0.340E_{c.m.})\ \text{MeV}, \tag{6}$$

in case of $\alpha + ^{46}$Ti. For $\alpha + ^{48}$Ti the corresponding energy dependence was

$$V_R = (151.8 - 0.307E_{c.m.})\ \text{MeV}. \tag{7}$$

It should, however, be pointed out that in order to arrive at eq. (6) we have employed the real part of the equivalent families at 45 and 50 MeV.

For the imaginary part of the optical potential the energy dependence turns out to be of the form

$$V_I = (12.1 + 0.082E_{c.m.})\ \text{MeV}, \tag{8}$$

$$V_I = (12.3 + 0.084E_{c.m.})\ \text{MeV}, \tag{9}$$

for $\alpha + ^{46}$Ti and $\alpha + ^{48}$Ti, respectively. It should be pointed out that to obtain eqs. (8) and (9) we have used the imaginary parts of the potential that were obtained by fine-tuning the corresponding parameters to fit our data extracted from systematics of the volume integrals (see table II).

3·2. *Inelastic scattering.* – The measured inelastic-scattering angular distributions to the first excited state of ^{46}Ti at 0.889 MeV with spin 2^+ at $E_\alpha = 45$ and 50 MeV are shown in fig. 7. These data were analysed in terms of collective model using DWBA. The distorted waves were generated by the optical potential ($m = n = 1$) deduced from the elastic data (see table I). The DWBA calculations were carried out by computer code DWUCK4 [13]. The calculations reproduce the data very well, more or less over the entire angular range at $E_\alpha = 45$ MeV and 50 MeV. The analysis yielded values of the $|\beta_2| = 0.24$ and 0.23 at $E_\alpha = 45$ and 50 MeV, respectively. Rebel *et al.* [2] obtained $\beta_2 = 0.236 \pm 0.005$ from folding model at $E_\alpha = 104$ MeV. The Saclay group [14] reported $|\beta_2| = 0.22$ at $E_\alpha = 44$ MeV (as obtained from the quoted deformation lengths).

For the first 2^+ excited state of ^{48}Ti at 0.983 MeV, the measured angular distributions at $E_\alpha = 40$ and 45 MeV are shown in fig. 8. At $E_\alpha = 40$ MeV the DWBA calculations reproduce the data quite well up to $\sim 80°$. Beyond this angle, the calculated cross-sections are somewhat higher (see fig. 8). This analysis yielded a value of the $|\beta_2| = 0.20$. For $E_\alpha = 45$ MeV the data were on the whole well described by the DWBA calculations (see fig. 8) and the comparison yielded a value of $|\beta_2| = 0.19$. The Saclay group [14] reported a value $\beta_2 = 0.18$ (as obtained from the quoted deformation lengths) at $E_\alpha = 44$ MeV. The β_2 values agreed very well with the ones reported in the literature [2-4, 14].

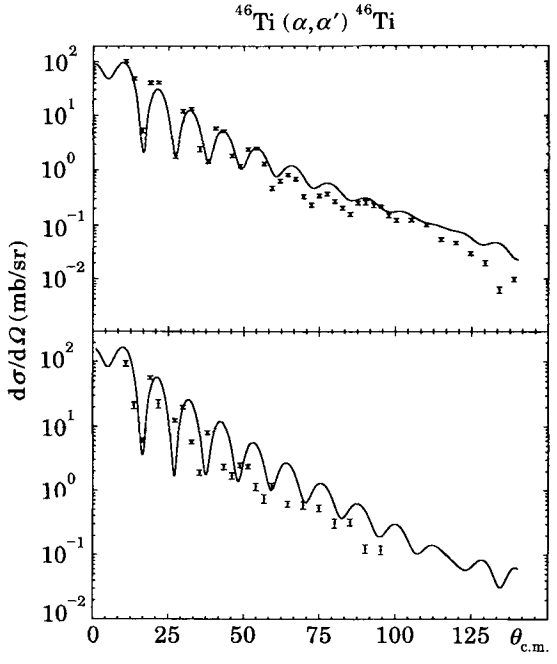

Fig. 7. – Inelastic-scattering cross-sections to the 0.889 MeV, 2^+ state of ^{46}Ti plotted as a function of the centre-of-mass angle. The full curves are calculated using the DWBA formalism. Top $E_\alpha = 45$ MeV, bottom $E_\alpha = 50$ MeV.

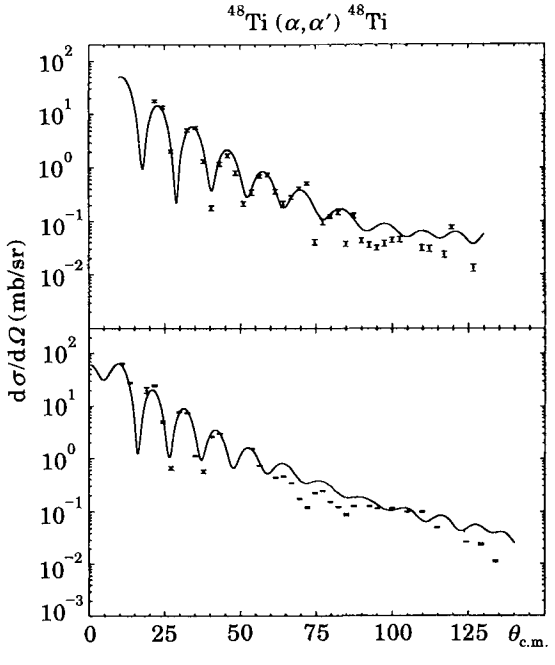

Fig. 8. – Inelastic-scattering cross-sections to the 0.983 MeV, 2^+ state of ^{48}Ti plotted as a function of the centre-of-mass angle. The full curves are calculated using the DWBA formalism. Top $E_\alpha = 40$ MeV, bottom $E_\alpha = 45$ MeV.

4. – Conclusion.

The elastic-scattering angular distributions of alpha-particles from ^{46}Ti at 45 MeV can be represented quite well beyond $\sim 60°$ by the standard optical potential and at 50 MeV more or less in the entire angular range of the data. At 45 MeV the Woods-Saxon squared for both the real and imaginary parts represents the data best, whereas at 50 MeV Woods-Saxon real and Woods-Saxon squared for the imaginary part provide the best representation. In case of ^{48}Ti at 40 MeV the standard optical model describes the data well up to $\sim 60°$ or so, and at 45 MeV in the entire angular range. On the other hand, at 40 MeV the non-standard form of the real part as Woods-Saxon squared and imaginary part as simple Woods-Saxon, and both parts as Woods-Saxon squared gave equally good fits, which were better than those given by the standard form. At 45 MeV, of course, both real and imaginary parts of the optical potential as Woods-Saxon squared gave by far the best description of the data. Thus the present data favour these types of potentials and draw further support for their employment from the analysis done in the past [4-8].

The notch perturbation test reveals that the sensitive region of the potential for predicting the elastic scattering is from 4 to 7 fm which is within the strong-absorption radii of ~ 7.4–7.5 fm for ^{46}Ti and ~ 7.64 for ^{48}Ti.

The present data allow four each at $E_\alpha = 45$ MeV and 50 MeV for ^{46}Ti, and three at $E_\alpha = 40$ MeV, and five at $E_\alpha = 45$ MeV for ^{48}Ti as the acceptable potential families.

The DWBA calculations describe the inelastic data on both the nuclei well. The values of deformation parameter β_2 agree very well with the ones reported in the literature for both the nuclei.

* * *

The authors are thankful to the staff of the Variable Energy Cyclotron Centre for providing the beam and other facilities including the detectors and electronics etc. for carrying out these measurements. They thank Dr. D. T. Khatting and Mr. P. Srinivas for their help during the experiment. They are grateful to Dr. H. J. Maier (University of Munich) for providing the targets. R. Singh gratefully acknowledges the financial assistance from the University Grants Commission (UGC), New Delhi in the form of a research project approved by the National Accelerator Users Committee of the UGC. One of us (VRR) thanks Council of Scientific and Industrial Research, New Delhi, for providing financial assistance in the form of an individual fellowship during his PhD period. Another one of us (MS) thanks North-Eastern Hill University for the fellowship awarded to him.

REFERENCES

[1] B. FERNANDEZ and J. S. BLAIR: *Phys. Rev. C*, **1**, 523 (1970).
[2] H. REBEL, G. HAUSER, G. W. SCHWEIRNER, G. NOWCKI, W. WIESNER and D. HARTMANN: *Nucl. Phys. A*, **218**, 13 (1974).
[3] J. L. YNTEMA and G. R. SATCHLER: *Phys. Rev.*, **161**, 1137 (1967).
[4] P. L. ROBERTSON, D. A. GOLDBERG, N. S. WALL, L. W. WOO and H. L. CHEN: *Phys. Rev. Lett.*, **42**, 54 (1979).

[5] V. RAGHUNATHA RAO, M. SUDARSHAN, A. SARMA, R. SINGH, S. R. BANERJEE and S. N. CHINTALAPUDI: *J. Phys. G*, **16**, 1861 (1991).
[6] TH. DELBAR, GH. GREGOIRE, G. PAIC, R. CEULENEER, F. MICHEL, R. VANDERPOORTEN, A. BUDZANOWSKI, H. DABORWSKI, L. FREINDL, K. GROTOWSKI, S. MICEK, R. PLANETA, A. STRAZALKOWSKI and K. A. EBERHARD: *Phys. Rev. C*, **18**, 1237 (1978).
[7] H. P. GUBLER, U. KIEBELE, H. O. MEYER, G. R. PLATTNER and I. SICK: *Nucl. Phys. A*, **351**, 29 (1981).
[8] R. PESL, H. J. GILLS, H. REBEL, E. FRIEDMANN, J. BUSCHMANN, H. KLEWEE-NEBENIUS and S. Z. ZAGROMSKI: *Z. Phys. A*, **313**, 111 (1983).
[9] S. K. GUPTA and K. H. W. MURTHY: *Z. Phys. A*, **307**, 187 (1982); A. SRIDHAR, N. LINGAPPA, S. K. GUPTA and S. KAILAS: *Phys. Rev. C*, **30**, 1760 (1984).
[10] A. CHATTERJEE, S. K. GUPTA, S. KAILAS and S. S. KEREKATTE: *Phys. Rev. C*, **37**, 1420 (1988).
[11] J. G. CRAMER and R. M. DE VRIES: *Phys. Rev. C*, **22**, 91 (1980).
[12] H. P. GUBLER, U. KIEBELE, H. O. MEYER, G. R. PLATTNER and I. SICK: *Phys. Lett. B*, **74**, 202 (1978).
[13] P. D. KUNZ:internal report, University of Colorado (unpublished) (1982).
[14] G. BRUGE, I. C. FAIURE, H. FARRAGI and A. BUSSIERE: *Nucl. Phys. A*, **146**, 597 (1970).